Strain-induced dimensional phase change of graphene-like boron nitride monolayers

Strain-induced dimensional phase change of graphene-like boron nitride monolayers

Qing Peng[*1,2,3]

E-mail: qpeng.org@gmail.com

Abstract. We investigate the coupling between the electronic bandgap and mechanical loading of graphene-like boron nitride (*h*-BN) monolayers up to failure strains and beyond by means of first-principles calculations. We reveal that the kinks in the bandgap-strain curve are coincident with the ultimate tensile strains, indicating a phase change. When the armchair strain is beyond the ultimate tensile strain, *h*-BN fails with a phase transformation from 2D honeycomb to 1D chain structure, characterized by the "V"-shape bandgap-strain curve. Large biaxial strains can break the 2D honeycomb structures into 0D individual atoms and the bandgap closes.

† [1] *Address, Nuclear Engineering and Radiological Sciences, University of Michigan, Ann Arbor, MI 48109, U.S.A.*

† [2] *Address, Department of Mechanical, Aerospace and Nuclear Engineering, Rensselaer Polytechnic Institute, Troy, NY 12180, U.S.A.*

† [3] *Address, School of Power and Mechanical Engineering, Wuhan University, Wuhan, 430072, China*

1. INTRODUCTION

Materials are vulnerable to strain, which ubiquitously exist both locally and globally. Strain could be introduced, both intentionally and unintentionally, by mechanical loading, vibration, thermal fluctuations, and defects [1, 2, 3]. The strains could be detrimental to the integrity of devices and degradation of material properties. It could also be beneficial, for instance, in tailoring material properties. Nowadays strain-engineering is a common approach to tune the electronic structure of nanomaterials [4, 5, 6, 7, 8, 9, 10, 11, 12, 13, 14]. A direct-indirect band gap transition has been induced by strain-engineering in two-dimensional phosphorene [15]. Strain-engineering technique is important for advanced logic technologies [16, 17]. By straning silicon, a leading-edge 90-nm technology had been reported [18, 19]. Strain engineering is a routine technique to enhance the carrier mobility in nanoscale MOSFETs [20].

Engineered by Strain, a room temperature semiconductor-metal transition has been achieved in MoTe2 thin films [21] and single-crystal vanadium dioxide beams [22].

Nano devices such as nano surface acoustic wave sensors and nano waveguides could be synthesized by introducing local strain [23, 24]. Management of the electronic performance under various large strains is vital and challenging in designing flexible electronics [25], where a precondition is the knowledge of the coupling effect of the mechanical and the electronic properties.

The graphene-like hexagonal boron nitride monolayer (*h*-BN) is a 2D nanomaterial analog of graphene having a honeycomb lattice structure [26]. *h*-BN is chemically inert, with a high thermal conductivity and resistant to oxidation. Due to its outstanding properties, *h*-BN has found wide applications in micro and nano-devices such as insulators with high thermal conductivity in electronic devices [26], ultraviolet-light emitters in optoelectronics [27, 28, 29, 30], and as nano-fillers in high strength and thermal conductive nanocomposites [31, 32]. It has been shown that a tunable band gap nanosheet can be constructed by fabrication of hybrid nanostructures made of graphene/*h*-BN domains [33], which opens a new venue for research in the application of *h*-BN for electronics [34].

Knowing the elastic properties, including elastic limits, is critical in design and practical applications [3]. It has reported that the *h*-BN monolayer has a bulk modulus around 160 GPa and a bending modulus around 31.2 GPa [26, 35]. The linear and non-linear (up to fifth order elastic constants) elastic properties of *h*-BN are reported in our previous study [36], as well as the effects of mechanical strains on its radiation hardness [37]. Due to the importance, the strain engineered bandgaps of *h*-BN have been extensively studied [38, 39, 40, 41, 42, 43]. The novelty of this study is the coupling between bandgap and mechanical strain at large strains with the exploring of subsequent phase changes, which manifests the upper limits of strain engineering of *h*-BN . Using high fidelity *ab initio* Density Functional Theory (DFT) calculations, we investigate the coupling between the mechanical and electronic properties at large tensile strains. To include more phonon modes into the model in addition to reducing the self-

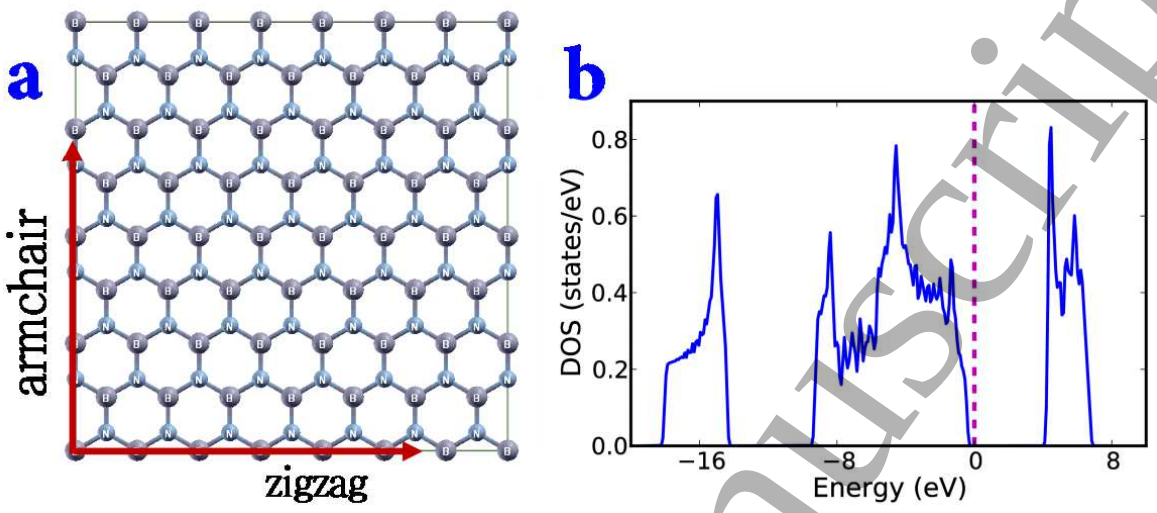

Figure 1. Geometry and DOS (a) The strain-free configuration of atomic super cells of 112 lattice sites of *h*-BN monolayer. The big balls denote B atoms and small balls denote N atoms. The armchair and zigzag directions are orthogonal, pointing to the nearest neighbor and the second nearest neighbor respectively. (b) The electronic density of states of the 112-atom super cell at strain-free configuration.

image interaction, we use a relatively larger simulation box containing 112 atoms. The details of the computational methods are in the Supplementary Information. We find a positive correlation between the strain and the electronic bandgap. We observe the phase transition from a 2D honeycomb to 1D chains and 0D atom dots. Our results provide theoretical limits for the strain-engineering of electronic properties in *h*-BN based van der Waals electronics.

2. SIMULATION METHOD

2.1. Mechanical Loading

When a macroscopically homogeneous deformation (deformation gradient tensor [44] $\mathbf{F}$) is applied, the lattice vectors of the deformed *h*-BN are $\mathbf{h}_i = \mathbf{F}\mathbf{H}_i$, $i = 1, 2, 3$, where $\mathbf{H_i}$ are lattice vectors of undeformed (reference) configuration. The Lagrangian strain [45] is defined as $\boldsymbol{\eta}=\frac{1}{2}(\mathbf{F}^{\mathbf{T}}\mathbf{F}-\mathbf{I})$, where $\mathbf{I}$ is the identity tensor. The strain energy density has functional form of $\Phi = \Phi(\boldsymbol{\eta})$. The elastic properties of a material are determined from Φ, which is quadratic in strain for a linear elastic material. Nonlinear elastic constitutive behavior is established by expanding Φ in a Taylor series in terms of powers of strain $\boldsymbol{\eta}$ (e.g. [46]).

In this study, we modeled the monolayer *h*-BN as a two dimensional (2-D) structure and assumed that the deformed state of the monolayer *h*-BN is such that the contribution of bending to the strain energy density is considered negligible, compared to the in-plane strain contribution. This assumption is reasonable since the radius of curvature of out-of-

plane deformation is Significantly larger than the in-plane inter-atomic distance. Then the stress state of the monolayer h-BN under those assumptions can be assumed to be 2-D and we only consider the in-plane stress and strain components for the structures studied.

We used a super cell with periodic boundary condition for the study of h-BN monolayer. The super cell contains 112 lattice sites in one plane. It is carefully selected to be nearly square, 17.601×17.421 Å, with x axis (direction 1) along zigzag direction and y axis (direction 2) along armchair direction. With such configuration, the deformation along two directions, 1 and 2, are similar.

Due to the periodic boundary condition, the defects in the self images may have Significant interactions with each other. To ensure that the interactions between self images are considered negligible, the distance between the nearest self images is set at 17.421 Å. The undeformed reference configurations of 112 lattice sites of h-BN are shown in Figure 1 in the main text.

Due to the anisotropy of the atomic structure, h-BN monolayers show different properties along different directions, typically armchair and zigzag directions. For a complete study, we applied strains to the h-BN monolayers in three modes as uniaxial strain along zigzag (z) and armchair (a) directions, and equal bi-axial strains along both directions on the prismatic plane (b).

The deformations of the system are applied by a strain tensor, with a corresponding deformation gradient on the supercell. Strain tensors in z, a, b are:

$$\begin{aligned} \mathbf{S}_z &= \begin{bmatrix} 1+\eta & 0 & 0 \\ 0 & 1 & 0 \\ 0 & 0 & 1 \end{bmatrix}, \mathbf{S}_a = \begin{bmatrix} 1 & 0 & 0 \\ 0 & 1+\eta & 0 \\ 0 & 0 & 1 \end{bmatrix}, \\ \mathbf{S}_b &= \begin{bmatrix} 1+\eta & 0 & 0 \\ 0 & 1+\eta & 0 \\ 0 & 0 & 1 \end{bmatrix}, \end{aligned} \tag{1}$$

where η is Lagrangian elastic strain [47]. The corresponding deformation gradient tensors [44] are :

$$\mathbf{F}_z = \begin{bmatrix} \varepsilon & 0 & 0 \\ 0 & 1 & 0 \\ 0 & 0 & 1 \end{bmatrix}, \mathbf{F}_a = \begin{bmatrix} 1 & 0 & 0 \\ 0 & \varepsilon & 0 \\ 0 & 0 & 1 \end{bmatrix}, \mathbf{F}_b = \begin{bmatrix} \varepsilon & 0 & 0 \\ 0 & \varepsilon & 0 \\ 0 & 0 & 1 \end{bmatrix}, \tag{2}$$

where ε is the stretch ratio. Taking case z as an example, the length of supercell in zigzag direction is εl_0, where l_0 is the length at strain free state. The length of supercell in other two directions will not change. ε is determined by the Lagrangian elastic strain [47] through equation $\varepsilon = \sqrt{1-2\eta}$.

For h-BN monolayer, the two-dimensional Young's modulus is defined as :

$$Y_{2D} = \frac{1}{A_0} \frac{\partial^2 E_s}{\partial \eta^2}|_{\eta=0}, \tag{3}$$

where E_s is the total strain energy, which is the addition of the total energy caused by strain, and A_0 is the equilibrium surface area at strain free state. More details of the mechanical loadings have been reported in our previous work [36], which have been well used to explore the mechanical properties of 2D materials [48, 49, 50, 51, 52, 53, 54, 55, 56, 57, 58, 59].

2.2. Density Functional Theory Calculations

The stress-strain relationship of *h*-BN monolayer under the desired deformation configurations are characterized via *ab initio* calculations with the density-functional theory (DFT). DFT calculations were carried out with the Vienna Ab-initio Simulation Package (VASP) [60, 61, 62, 63] which is based on the Kohn-Sham Density Functional Theory (KS-DFT) [64, 65] with the generalized gradient approximations as parameterized by Perdew, Burke and Ernzerhof (PBE) for exchange-correlation functions [66]. The electrons explicitly included in the calculations are the ($2s^2 2p^1$) electrons of boron and ($2s^2 2p^3$) electrons of nitrogen. The core electrons ($1s^2$) of boron and nitrogen are replaced by the projector augmented wave (PAW) and pseudo-potential approach [67, 68]. A plane-wave cutoff of 400 eV is used in all the calculations. The calculations are performed at zero temperature.

The criterion to stop the relaxation of the electronic degrees of freedom is set by the total energy change to be smaller than 0.00001 eV. The optimized atomic geometry was achieved through minimizing Hellmann-Feynman forces acting on each atom until the maximum forces on the ions were smaller than 0.01 eV/Å.

The atomic structures of all the deformed and undeformed configurations are obtained by fully relaxing a 112-atom-unit cell where all atoms were placed in one plane. The simulation invokes periodic boundary conditions for the two in-plane directions while the displacement to out-of-plane direction is forbidden.

The irreducible Brillouin Zone was sampled with a Gamma-centered 5×5×1 *k*-mesh. Such dense *k*-mesh was selected to ensure the energy convergence to 1 meV, reduce the numerical errors caused by the strain of the systems. The initial charge densities were taken as a superposition of atomic charge densities. There was a 15 Å thick vacuum region to reduce the inter-layer interaction to model the single layer system. The results of the calculations are independent of the precise value of the out-of-plane thickness, so there is no physical interpretation attached to the quantity.

The VASP simulation calculates the true or Cauchy stress, $\mathbf{\Sigma}$, which for monolayer *h*-BN must be expressed as a 2D force per length with units of N/m by taking the product of the Cauchy stress (with units of N/m^2) and the super-cell thickness of 15 Å. The Cauchy stress is related to the second Piola-Kirchhoff (PK2) stress Σ as: [46]

$$\mathbf{\Sigma} = \boldsymbol{J}\mathbf{F}^{-1}\boldsymbol{\sigma}(\mathbf{F}^{-1})^{\boldsymbol{T}} \tag{4}$$

where J is the determinant of the deformation gradient tensor $\mathbf{F}$ in Eqn. 2.

3. RESULTS AND ANALYSIS

The fully relaxed geometry of the whole 112-atom supercell is shown in Fig. 1 with the simulation box and orientations. All atoms are coplanar. The lattice constant of the *h*-BN monolayer at strain free state is 2.512 Å, in good agreement with experiment (2.51 Å) [69, 70] and DFT calculations [71, 40, 41]. The electronic properties are extensively studied [72]. It is well known that *h*-BN monolayers are insulators with a wide indirect bandgap [73]. Interested readers could refer to the details of the electronic band structures of the *h*-BN monolayers, for example ref. [74] of our previous study. The electronic density of states of the strain-free state of *h*-BN monolayers represented in the 112-atom simulation box in this study are explicitly illustrated in Fig. 1(b), serving as a reference to the strained states discussed later. The valence band maximum (VBM) is set to be zero and marked as a dashed line. The bandgap is 4.6 eV, agreeing well with previous DFT studies [40, 41].

It is worth noting that our result of the bandgap is about 25% lower than the value of 6.17 eV reported by an experimental investigation [75]. The discrepancy is attributed to the employed generalized gradient approximations of the exchange-correlation functionals, which does not accurately capture the discontinuous energy change associated with electron transfer. More accurate quasi-particle methods are available [76] but it is impractical for large systems limited by computing power. Although the predicted bandgap of an individual configuration is inaccurate, the trend of the bandgap variation could be accurately captured [77]. Therefore, we only consider the trends of band gaps under the mechanical strain loading, and do not make precise bandgap predictions at any individual system.

When the strains are applied, all the atoms are fully relaxed. We studied the behavior of the system under the strain that ranged from 0 to 0.4, with an increment of 0.02 in each step for all three deformation modes. All strains are expressed in the form of Lagrangian (true) strain. Such a wide range is carefully selected so that the deformations beyond failure can also be theoretically investigated. It is worth noting that although these large mechanical loading beyond failure are infeasible in any real experiments, it is still valuable in providing insights and theoretical up-boundary.

The stress-strain relationship of three strain modes are shown in Fig. 2. For the zigzag mode (z mode), the stress in the zigzag direction increases from 0 to the maximum of 27.08 N/m, which is the ultimate tensile strain. The corresponding strain, namely ultimate tensile strain, is 0.24. Beyond the ultimate tensile strain, the stress monotonically decreases. The band gap decreases monotonically with respect to tensile strain (Fig. 2b). There is a turn in the strain of 0.24, with a band gap of 3.8 eV. When the tensile strain is less than 0.24, the band gap decrease nearly linearly with an increasing strain, and the speed of the change of the band gap is much slower than that beyond the ultimate tensile strain. The electronic band gap as a function of strain can be expressed by the relationship of $E_g = -3.3\eta^z + 4.6$ eV for strain in range $0 \leq \eta^z \leq 0.24$, where η^z is the Lagrangian strain in the zigzag direction. Beyond the ultimate tensile

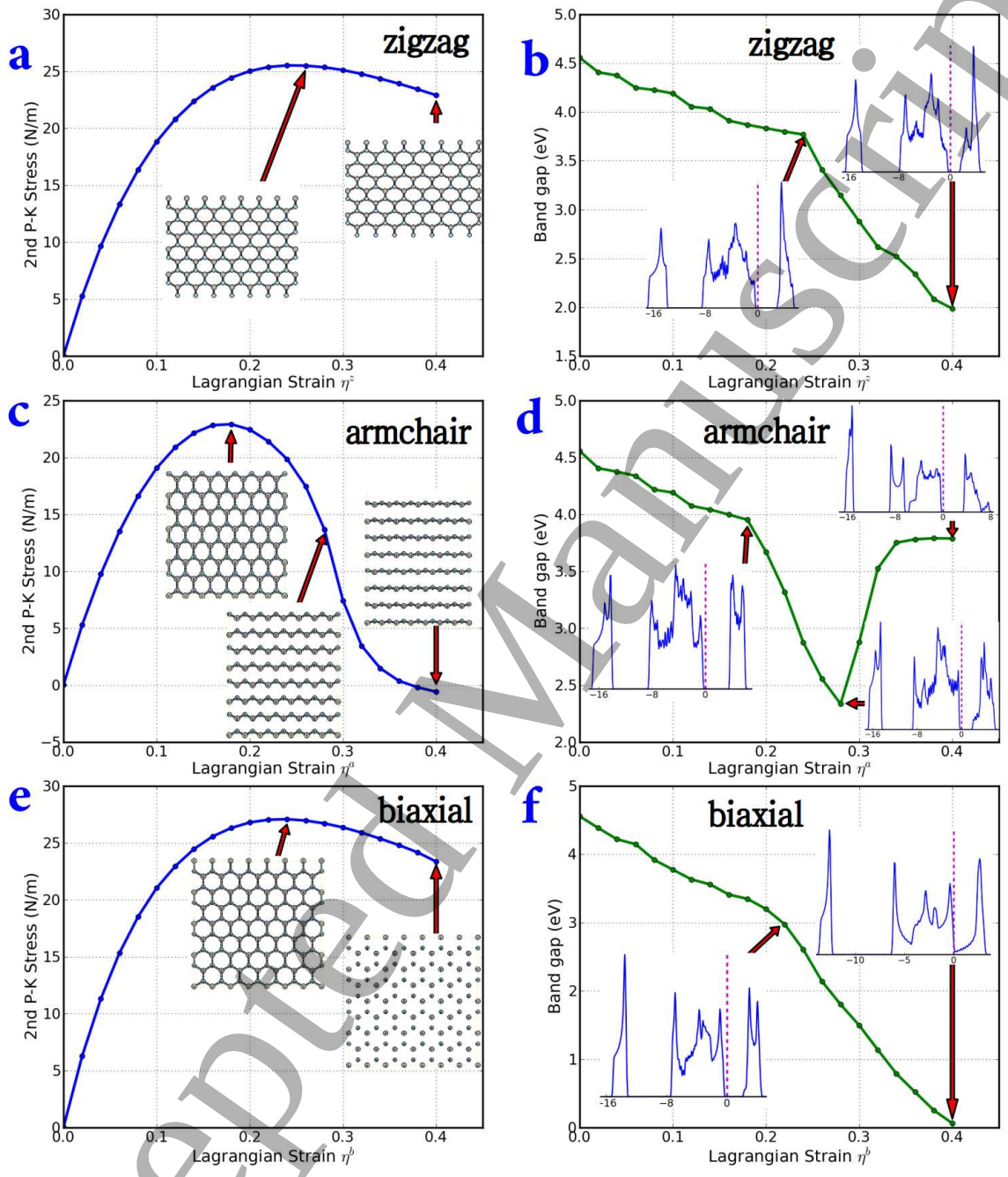

Figure 2. Mechanic/electronic coupling The stress-strain curve of three tensile strain modes along the (a) zigzag, (c) armchair, (e) biaxial directions in the plane. The "2nd P-K stress" denotes the second Piola-Kirchhoff stress. The insets are the geometry snapshots at the ultimate tensile strains and beyond. The electronic band gap as a function of mechanical strains along (b) zigzag, (d) armchair, (f) biaxial direction in the plane. The insets are the electronic density of states at the ultimate tensile strains and beyond.

strain, the function becomes $E_g = -11.25\eta^z + 6.5$ eV. The decreasing speed is three times faster than that before the ultimate tensile strain. Our results of the variation of the bandgap agree well with the previous study [39].

The stress-strain response of the armchair mode (a mode) is very different to that of z mode, as the following four aspects. First, the ultimate tensile stress 24.48 N/m is smaller than that of zigzag mode (27.08 N/m). Second, the ultimate tensile strain 0.18 is much smaller than that of zigzag mode (0.24). Third, the tensile stress decreases rapidly beyond the ultimate tensile stress. Fourth, the tensile stress turns from positive to negative, indicating severe material failure, which is evident from the snapshots of the geometries in the insets.

The corresponding electronic structures have also distinctive features in the armchair deformation than that of zigzag. The most prominent feature is that the "V"-shape of the bandgap-strain curve. At the strain of 0.28, there is a minimum of 2.3 eV in the bandgap-strain curve, and we denote this strain as "valley" strain. The bandgap linearly decreases with respect to strain before the ultimate tensile strain 0.18, with the relationship of $E_g = -3.61\eta^a + 4.6$ eV, where η^a is the Lagrangian strain in the armchair direction. The slope in this regime is similar to that in the zigzag mode. However, the decreasing speed is much faster beyond the ultimate tensile strain. The variation of the bandgap follows the function of $E_g = -16.5\eta^a + 6.9$ eV for $0.18 \leq \eta^a \leq 0.28$. For the strains beyond the valley strain 0.28, the band gap increases with an increasing tensile strain. This behavior is strikingly distinguishable from previous investigations. This abnormal overturn of the trend of bandgap variation at the valley strain implies significant structure change. It can be clearly seen that the two-dimensional planar honeycomb structure now turns into parallelled one-dimensional B-N chains, as illustrated in the insets in Fig. 2d. In other words, there is a structural phase transition from a 2D honeycomb to 1D chains.

The 1D BN chains still interact with each other after the phase transition. Once the strain increases beyond the valley strain of 0.28, the separation of these paralleled 1D BN chains increases and the coupling between these chains becomes weaker. When the strain is 0.34 and above, there is a plateau of the bandgap, which indicates that the 1D BN chains are well separated from each other.

The shape of the stress-strain curve of biaxial mode (b mode) deformation is alike to that of the z mode. The ultimate tensile strength is 28.64 N/m and the corresponding ultimate tensile strain is 0.24. The stress decreases slowly with respect to the biaxial strain. The snapshot of the geometry in the insets of Fig. 2e shows that the h-BN structure is well kept for $\eta^b < 0.24$. However, the h-BN monolayer fails for strains larger than 0.24. The system eventually becomes individual atoms that are well separated (inset in Fig. 2e). This structure phase change can be captured by the change of the bandgaps. The bandgap decreases when the applied biaxial tensile strain increases. The bandgap closes up at the strain of 0.4. The bandgap-strain curve shows that there is a kink at the strain of 0.22, a small value (0.02) deviated from the ultimate tensile strain of 0.24 due to numerical errors. It is worth noting that the ultimate

Table 1. Ultimate tensile strain η_u and the first kink strain η_k of *h*-BN in three deformation modes. The first kink strain is the corresponding strain that the first kink in a bandgap curves (electronic bandgap energy as a function of strain) occurs.

	zigzag	armchair	biaxial
η_u	0.24	0.18	0.24
η_k	0.24	0.18	0.22

tensile strain extrapolated from nanoindentation experiment on a few layers (about two layers) *h*-BN is 0.22 [69], agreeing well with our mechanical prediction of 0.24 from the stress-strain curve and electronic prediction of 0.22 from the bandgap-strain curve.

The speed of the reduction of bandgap as a function of strain is slow when the strain is smaller than ultimate tensile strain, and faster when the strain is more than 0.22. The first part of the bandgap curve obeys the equation $E_g = -7.3\eta^b + 4.6$ eV for $0 \leq \eta^b \leq 0.22$, where η^b is the Lagrangian strain in the biaxial direction. The second part of the bandgap curve can be described by the function $E_g = -16.7\eta^b + 6.7$ eV. At the strain of 0.4, the 2D *h*-BN structure breaks up and forms individual atoms. We can still consider this as a phase change, from two-dimensional to zero dimensional. It is worth pointing out that this phase change 2D→0D is similar to the phase change of 2D→1D in uniaxial armchair deformation. It is interesting that the bandgap shapes are similar in both phase change paths, since the slope of the bandgap-strain curve in biaxial deformation is almost the same as that in the uniaxial deformation along armchair direction. Our results of the bandgap changes with respect to the three deformation modes agree well with the previous DFT study [39].

With an overview of all the three representative deformation modes, one could conclude that the bandgaps decrease with respect to an increasing tensile strain. The strain-engining bandgap is efficient because the significant amount of the bandgap reduction could be achieved. The integrity of the *h*-BN monolayers becomes vulnerable when the mechanical strains are higher than the ultimate tensile strains. For the uniaxial deformation along the armchair direction, there is a kink in the bandgap-strain curve, which is coincident with the ultimate tensile strain. Beyond the ultimate tensile strain, the system experiences a phase change from 2D to 1D for strains, clearly marked is the "V"-shape of the bandgap-strain curve. For biaxial deformation, the system fails at the ultimate tensile strain, starting with the phase transformation from 2D to 1D and forming individual atoms. The clear mark is the bandgap closeup in the bandgap-strain curve. When the strain is smaller than the ultimate strain, the speed of the reduction of the bandgap as a function of strain is much smaller than that when the stain is larger than the ultimate tensile strain.

Our striking result is the strain induced phase transitions could be marked in the bandgap-strain curves of *h*-BN monolayer. There is a positive correlation between the stress-strain curves and bandgap-strain curves. For example, Table 1 illustrates the strong correlation between the ultimate tensile strain and the first kink strain.

Such a strong and positive correlation manifests the strong coupling effect between the mechanical properties and electronic properties. Our results of the coupling effect of mechanical and electronic properties could provide a guide for the strain-engineering of *h*-BN based electronics. In addition, our results show that the 1D BN chains could be fabricated by the micromechanical peeling of 2D honeycomb BN, similar to the peeling of 3D hexagonal BN for 2D structures. Furthermore, 0D BN structures could also be achieved by "mechanical" decomposition under large biaxial strains.

Our investigation extends the range of strain of previous studies [73, 74, 76, 39]. With the examination of large strains, our theoretical study explored the upper limits of strain in strain engineering, which is unreachable by experimental approaches. For more accurate modeling of the instablility at large strain, we used a large supercell to include the phonons with short wavelength, which are missed in previous studies [73, 74, 76, 39]. It is worth noting that all the calculations are performed at zero temperature to suppress the kinetics and thermodynamics effects which are inevitable in the real experiments at finite temperature. Our theoretical investigation is valuable because it provides an upper limit for the experiments and explored the strain domains that otherwise limited by experiments. Since the method of first-principles calculations are well established and robust, our results are reliable and could serve as a guidance for future experimental investigations, manifesting the beauty and advantage of the theoretical investigation.

4. CONCLUSION

In summary, we studied the mechanical failure and the variation of the electronic properties in response to the mechanical loading in monolayer hexagonal boron nitride through first-principles calculations. Three typical strain fields were applied: uniaxial along zigzag, armchair directions and equibiaxial in plane. Large mechanical strains are applied way beyond the failure. Our results shows that mechanical strains, either uniaxial or biaxial, can diminish the bandgap width efficiently. We observed the correlation between the kink in the bandgap-strain curve and the ultimate tensile strain. Beyond the failure strain, we observed phase transitions. Particularly, when the armchair strain is beyond the ultimate tensile strain, *h*-BN fails with a phase transformation from 2D honeycomb to 1D chain structure. This phase change is characterized by the "V"-shape bandgap-strain curve. Furthermore, large biaxial strains can cause the phase change from the honeycomb structures into individual atoms and the bandgap closes. Our results of the electronic-mechanical coupling and phase changes could serve as a roadmap for strain engineering the electronic properties for *h*-BN based flexible electronics.

References

[1] Di Fonzo S, Jark W, Lagomarsino S, Giannini C, De Caro L, Cedola A and Muller M 2000 *Nature* **403** 638–640 ISSN 0028-0836

[2] Liu F, Rugheimer P, Mateeva E, Savage D E and Lagally M G 2002 *Nature* **416** 498–498 ISSN 0028-0836

[3] Lee C, Wei X, Kysar J W and Hone J 2008 *Science* **321** 385–388

[4] OREILLY E 1989 *SEMICONDUCTOR SCIENCE AND TECHNOLOGY* **4** 121–137 ISSN 0268-1242

[5] Mei Y, Huang G, Solovev A A, Urena E B, Moench I, Ding F, Reindl T, Fu R K Y, Chu P K and Schmidt O G 2008 *ADVANCED MATERIALS* **20** 4085+ ISSN 0935-9648

[6] Feng J, Qian X, Huang C W and Li J 2012 *NATURE PHOTONICS* **6** 865–871 ISSN 1749-4885

[7] Fei R and Yang L 2014 *NANO LETTERS* **14** 2884–2889 ISSN 1530-6984

[8] Pereira V M and Castro Neto A H 2009 *PHYSICAL REVIEW LETTERS* **103** ISSN 0031-9007

[9] Guinea F, Katsnelson M I and Geim A K 2010 *NATURE PHYSICS* **6** 30–33 ISSN 1745-2473

[10] Pereira V M and Castro Neto A H 2009 *Phys. Rev. Lett.* **103**(4) 046801

[11] Roldan R, Castellanos-Gomez A, Cappelluti E and Guinea F 2015 *JOURNAL OF PHYSICS-CONDENSED MATTER* **27** ISSN 0953-8984

[12] Si C, Sun Z and Liu F 2016 *NANOSCALE* **8** 3207–3217 ISSN 2040-3364

[13] Umeno Y, Shimada T, Kinoshita Y and Kitamura T 2017 Strain Engineering on Nanosemiconductors *MULTIPHYSICS IN NANOSTRUCTURES* Nanostructure Science and Technology pp 67–96 ISBN 978-4-431-56573-4; 978-4-431-56571-0

[14] Castellanos-Gomez A, Roldan R, Cappelluti E, Buscema M, Guinea F, van der Zant H S J and Steele G A 2013 *NANO LETTERS* **13** 5361–5366 ISSN 1530-6984

[15] Peng X, Wei Q and Copple A 2014 *PHYSICAL REVIEW B* **90** ISSN 1098-0121

[16] Thompson S, Sun G, Choi Y and Nishida T 2006 *IEEE TRANSACTIONS ON ELECTRON DEVICES* **53** 1010–1020 ISSN 0018-9383

[17] Sun Y, Thompson S E and Nishida T 2007 *JOURNAL OF APPLIED PHYSICS* **101** ISSN 0021-8979

[18] Thompson S, Armstrong M, Auth C, Alavi M, Buehler M, Chau R, Cea S, Ghani T, Glass G, Hoffman T, Jan C, Kenyon C, Klaus J, Kuhn K, Ma Z, Mcintyre B, Mistry K, Murthy A, Obradovic B, Nagisetty R, Nguyen P, Sivakumar S, Shaheed R, Shiften L, Tufts B, Tyagi S, Bohr M and El-Mansy Y 2004 *IEEE TRANSACTIONS ON ELECTRON DEVICES* **51** 1790–1797 ISSN 0018-9383

[19] Thompson S, Armstrong M, Auth C, Cea S, Chau R, Glass G, Hoffman T, Klaus J, Ma Z, Mcintyre B, Murthy A, Obradovic B, Shifren L, Sivakumar S, Tyagi S, Ghani T, Mistry K, Bohr M and El-Mansy Y 2004 *IEEE ELECTRON DEVICE LETTERS* **25** 191–193 ISSN 0741-3106

[20] Chu M, Sun Y, Aghoram U and Thompson S E 2009 *ANNUAL REVIEW OF MATERIALS RESEARCH* **39** 203–229 ISSN 1531-7331

[21] Song S, Keum D H, Cho S, Perello D, Kim Y and Lee Y H 2016 *NANO LETTERS* **16** 188–193 ISSN 1530-6984

[22] Cao J, Ertekin E, Srinivasan V, Fan W, Huang S, Zheng H, Yim J W L, Khanal D R, Ogletree D F, Grossmanan J C and Wu J 2009 *NATURE NANOTECHNOLOGY* **4** 732–737 ISSN 1748-3387

[23] Peng Q, Zamiri A R, Ji W and De S 2012 *Acta Mechanica* **223** 2591–2596

[24] Peng Q, Ji W and De S 2012 *Phys. Chem. Chem. Phys.* **14** 13385–13391

[25] Akinwande D, Petrone N and Hone J 2014 **5** 5678 EP –

[26] Nag A, Raidongia K, Hembram K P S S, Datta R, Waghmare U V and Rao C N R 2010 *ACS Nano* **4** 1539

[27] Suryavanshi A, Yu M, Wen J, Tang C and Bando Y 2004 *Appl. Phys. Lett.* **84** 2527

[28] Kim P, Shi L, Majumdar A and McEuen P L 2001 *Phys. Rev. Lett.* **87** 215502

[29] Blase X, Rubio A, Louie S G and Cohen M L 1994 *Europhys. Lett.* **28** 335

[30] Watanabe K, Taniguchi T and Kanda H 2004 *Nature Mater.* **3** 404

[31] Lee G W, Park M, Kim J, Lee J I and Yoon H G 2006 *Comosites Part A-Applied Science and Manufacturing* **37** 727

[32] Zhi C, Bando Y, Tang C, Kuwahara H and Golberg D 2009 *Advanced Materials* **21** 2889

[33] Zhong X, Yap Y K, Pandey R and Karna S P 2011 *Phys. Rev. B* **83**(19) 193403
[34] Ci L, Song L, Jin C, Jariwala D, Wu D, Li Y, Srivastava A, Wang Z F, Storr K, Balicas L, Liu F and Ajayan P M 2010 *Nat. Mater.* **9** 430–435
[35] Andrew R C, Mapasha R E, Ukpong A M and Chetty N 2012 *Phys. Rev. B* **85**(12) 125428
[36] Peng Q, Ji W and De S 2012 *Comput. Mater. Sci.* **56** 11 – 17
[37] Peng Q, Ji W and De S 2013 *Nanoscale* **5** 695–703
[38] Bernardi M, Palummo M and Grossman J C 2012 *Phys. Rev. Lett.* **108**(22) 226805
[39] Li J, Gui G and Zhong J 2008 *J. Appl. Phys.* **104** 094311
[40] Wu J, Wang B, Wei Y, Yang R and Dresselhaus M 2013 *Mater. Res. Lett.* **1** 200–206
[41] Jalilian J and Safari M 2016 *Diam. Relat. Mater.* **66** 163 – 170 ISSN 0925-9635
[42] Amorim R G, Zhong X, Mukhopadhyay S, Pandey R, Rocha A R and Karna S P 2013 *J. Phys. Condens. Matter* **25** 195801
[43] Huang Z, L T Y, Wang H Q, Yang S W and Zheng J C 2017 *Comput. Mater. Sci.* **130** 232 – 241 ISSN 0927-0256
[44] Crisfield M 1991 *Non-Linear Finite Element Analysis of Solids and Structures* (New York: John Wiley & Sons)
[45] Lubliner J 2008 *Plasticity Theory* (New York: Dover Publications)
[46] Wei X, Fragneaud B, Marianetti C A and Kysar J W 2009 *Phys. Rev. B* **80** 205407
[47] Brugger K 1964 *Phys. Rev. A* **133** 1611
[48] Peng Q, Liang C, Ji W and De S 2012 *Model. Numer. Simul. Mater. Sci.* **2** 76–84
[49] Peng Q, Liang C, Ji W and De S 2013 *Comput. Mater. Sci.* **68** 320–324
[50] Peng Q, Liang C, Ji W and De S 2013 *Phys. Chem. Chem. Phys.* **15**(6) 2003–2011
[51] Peng Q, Liang C, Ji W and De S 2013 *Mech. Mater.* **64** 135–141
[52] Peng Q, Chen Z and De S 2015 *Mech. Adv. Mater. Struc.* **22** 717–721
[53] Peng Q, Wen X and De S 2013 *RSC Adv.* **3** 13772 – 13781
[54] Peng Q and De S 2013 *Phys. Chem. Chem. Phys.* **15** 19427 – 19437
[55] Peng Q and De S 2013 *RSC Adv.* **3** 24337 – 24344
[56] Peng Q, Han L, Wen X, Liu S, Chen Z, Lian J and De S 2015 *Phys. Chem. Chem. Phys.* **17** 2160–2168
[57] Peng Q, Han L, Wen X, Liu S, Chen Z, Lian J and De S 2015 *RSC Adv.* **5** 11240–11247
[58] Peng Q, Dearden A K, Chen X J, Huang C, Wen X and De S 2015 *Nanoscale* **7** 9975–9979
[59] Peng Q, Han L, Lian J, Wen X, Liu S, Chen Z, Koratkar N and De S 2015 *Phys. Chem. Chem. Phys.* **17**(29) 19484–19490
[60] Kresse G and Hafner J 1993 *Phys. Rev. B* **47** 558
[61] Kresse G and Hafner J 1994 *Phys. Rev. B* **49** 14251
[62] Kresse G and Furthuller J 1996 *Phys. Rev. B* **54** 11169
[63] Kresse G and Furthuller J 1996 *Comput. Mater. Sci.* **6** 15
[64] Hohenberg P and Kohn W 1964 *Phys. Rev.* **136** B864
[65] Kohn W and Sham L J 1965 *Phys. Rev.* **140** A1133
[66] Perdew J P, Burke K and Ernzerhof M 1996 *Phys. Rev. Lett.* **77**(18) 3865–3868
[67] Blöchl P E 1994 *Phys. Rev. B* **50** 17953–17979
[68] Jones R O and Gunnarsson O 1989 *Rev. Mod. Phys.* **61** 689–746
[69] Song L, Ci L, Lu H, Sorokin P B, Jin C, Ni J, Kvashnin A G, Kvashnin D G, Lou J, Yakobson B I and Ajayan P M 2010 *Nano Lett.* **10** 3209–3215
[70] Liu L, Feng Y P and Shen Z X 2003 *Phys. Rev. B* **68** 104102
[71] Topsakal M, Aktürk E and Ciraci S 2009 *Phys. Rev. B* **79** 115442
[72] Pakdel A, Zhi C, Bando Y and Golberg D 2012 *Mater. Today* **15** 256 – 265 ISSN 1369-7021
[73] Wang J, Ma F, Liang W and Sun M 2017 *Mater. Today Phys.* **2** 6 – 34 ISSN 2542-5293
[74] Peng Q and De S 2012 *Physica E* **44** 1662–1666
[75] Ba K, Jiang W, Cheng J, Bao J, Xuan N, Sun Y, Liu B, Xie A, Wu S and Sun Z 2017 **7** 45584
[76] Shishkin M, Marsman M and Kresse G 2007 *Phys. Rev. Lett.* **99**(24) 246403

[77] Shen T, Penumatcha A V and Appenzeller J 2016 *ACS Nano* **10** 4712–4718

Acknowledgements

We thank Dr. Albert Dearden and Dr. Binghui Deng for the proof reading of the manuscript.

Additional information

Supplementary information is available in the online version of the paper. The SI includes details of the computational methods. Correspondence and requests for materials should be addressed to qpeng.org@gmail.com (Q.P.)

Competing financial interests

The authors declare no competing financial interests.